A Viscous Flow Solver for Time-Dependent Free Surface Calculations

Geoffrey W. Cowles

School for Marine Science and Technology
University of Massachusetts Dartmouth
New Bedford, MA 02744
Email: gcowles@umassd.edu

Luigi Martinelli

Mechanical and Aerospace Engineering
Princeton University
Princeton, NJ 08544

***Abstract*—In the present work, a robust and efficient algorithm for the computation of steady and time-dependent viscous fluid flow about advancing ships is developed. The baseline numerical algorithm couples the method of artificial compressibility with a finite volume cell-center discretization of the Reynolds-averaged Navier-Stokes equations. An efficient multigrid time-stepping scheme with residual smoothing and local time-stepping is implemented, resulting in an algorithm with fast convergence rates. Dual time-stepping is used to advance the system of equations in a time accurate manner. Fully nonlinear treatment of the wave field is provided by conforming the grid to the free surface shape. This core scheme is implemented for solution on parallel computers using the method of domain decomposition. The resulting computational tool is highly efficient and provides fast and accurate solutions of fluid flow about general hull shapes. Demonstration of the method for computation of the hydrodynamic forces on a Wigley hull in regular headwaves is presented.**

I. Introduction

The prediction of the resistance of a ship advancing through regular waves is a complex problem which requires a thorough understanding of the hydrodynamic forces acting on the ship hull, the physical processes from which these forces arise and their mutual interaction. The rise of affordable computational power has made possible computational solutions of the full set of mathematical equations which describe the coupled wave structure and viscous boundary layer interaction. Notable previous computational approaches in this area for computations of steady flow include the finite-difference, velocity-pressure coupling approach of Hino [1]; the finite-volume, velocity-pressure coupling approach of Miyata *et. al.* [2]; the interactive approach of Tahara *et. al.* [3] which used an interactive approach where the near field was computed using the RANS equations and the far field was treated using an inviscid formulation, and the fully viscous approach of Farmer [4]. Time-dependent calculations are traditionally made using approaches based on potential flow, including both strip theory (e.g. [5]) and panel methods (e.g. [6]). More recent efforts have focused on the computation of unsteady viscous flows using the Reynolds-averaged Navier-Stokes equations (e.g. [7]).

For computational techniques to be useful for naval architects, they must be fast, robust, and accurate. They also need to be applicable to realistic hull shapes ranging from naval combatant vessels to International America's Cup Class yachts. A critical timescale of the design process is the overnight turnaround which allows engineers to quickly evaluate the influence of hull modifications. Recent advances in adjoint based design for ships (e.g. [8]) have enabled extremely efficient automated shape optimizations of complex vehicles. Based on the application of control-theory to the solution of partial differential equations, such methods effectively eliminate the dependency of the computational cost of the optimization problem on the number of degrees of freedom of the design space. However, these design methods still require multiple flow solutions and thus rely strongly on an efficient core solver.

In this work we present an efficient method for computing time-dependent viscous flows around surface-piercing vessels. To overcome the difficulties preserving incompressibility, we cast the system of equations into a form suitable for time marching by using Chorin's method of artificial compressibility [9] whereby a time derivative of pressure is used to drive the continuity equation towards a steady state solution. To maintain a time accurate solution we utilize the method of dual time-stepping initiated by Peyret [10] and coupled with multigrid by Jameson [11]. In this approach, the discretization of the spatial and time derivatives are completely uncoupled, allowing for rapid modification of the temporal order of accuracy to adjust to problem stiffness. Dual time-stepping with multigrid has been utilized for a variety of applications, including coupled fluid-structure interaction [12], DNS simulations around bluff bodies using both structured [13] and unstructured grids [14]. The present solver uses a surface tracking method whereby the kinematic equation is explicitly solved and the mesh deforms to follow the time-dependent free surface. The entire flow solver is parallelized using a single program multiple data approach with MPI for rapid execution on modern clusters. The resulting solver is accurate and efficient enough to be used within the design process.

978-0-933957-40-4 ©2013 MTS

II. Mathematical Models

A. Coordinate System

Figure 1 shows the reference frame and computational domain used in this work. A right-handed coordinate system with the origin fixed at the intersection of the bow and the mean free surface is established. The z direction is positive upwards, y is positive towards the starboard side and x is positive in the downstream direction. Due to symmetry, only one half of the ship is considered.

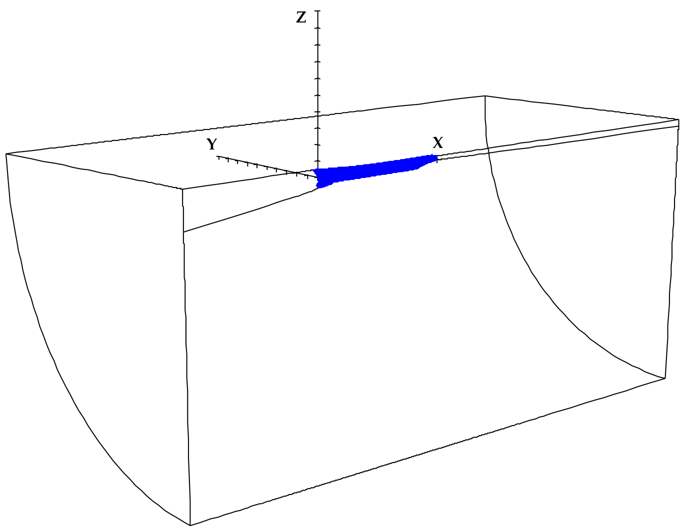

Fig. 1. Computational domain and coordinate system.

B. Governing Equations

For a viscous incompressible fluid moving under the influence of gravity, the differential form of the continuity equation and the Reynolds Averaged Navier-Stokes equations (RANS) in a Cartesian coordinate system can be cast, using tensor notation, in the form,

$$\frac{\partial \bar{U}_i}{\partial x_i} = 0 \tag{1}$$

$$\frac{\partial \bar{U}_i}{\partial t} + \bar{U}_j \frac{\partial \bar{U}_i}{\partial x_j} = -\frac{1}{\rho}\frac{\partial \bar{P}}{\partial x_j} + \frac{\partial}{\partial x_j}\left[\nu\left(\frac{\partial \bar{U}_i}{\partial x_j} + \frac{\partial \bar{U}_j}{\partial x_i}\right) - \overline{u_i u_j}\right] + \bar{F}_i. \tag{2}$$

Here, $\bar{U}_i$ is the mean velocity components in the x_i direction, $\bar{P}$, the mean pressure, $\bar{F}_i$ the gravity force acting in the i-th direction, and $\overline{u_i u_j}$ is the kinematic Reynolds stress which requires an additional model for closure. For implementation in a computer code, it is more convenient to use a dimensionless form of the equation which is obtained by dividing all lengths by the ship waterline length L and all velocity components by the free stream velocity U_∞. Moreover, one can define a new variable Ψ as the mean static pressure P minus the nondimensional hydrostatic component $-x_k Fr^{-2}$. For this work, the Reynolds stress is modeled using the algebraic Baldwin and Lomax turbulence model [15] which uses a turbulent eddy viscosity approach. The dimensionless form of the RANS becomes:

$$\frac{\partial u_i}{\partial x_i} = 0. \tag{3}$$

$$\frac{\partial u_i}{\partial t} + u_k \frac{\partial u_i}{\partial x_k} = -\frac{\partial \Psi}{\partial x_i} + \frac{\partial}{\partial x_k}\frac{1}{(Re_t)}\left(\frac{\partial u_i}{\partial x_k} + \frac{\partial u_k}{\partial x_i}\right) \tag{4}$$

where all velocities are normalized by the mean value of the streamwise velocity ($\bar{U}$), and lengthscales by the ship length L. This results in two key nondimensional numbers, the Froude number $Fr = \frac{U_\infty}{\sqrt{gL}}$ and the turbulent Reynolds number $Re_t = \frac{U_\infty L}{\nu_t}$ where ν_t is the turbulent kinematic eddy viscosity.

C. Free Surface Boundary Conditions

When the effects of surface tension and viscosity are neglected, the boundary condition on the free surface consists of two equations. The first, the dynamic condition, states that the pressure acting on the free surface is constant. The second, the kinematic condition, states that the free surface is a material surface: once a fluid particle is on the free surface, it forever remains on the surface. The dynamic and kinematic boundary conditions may be expressed as

$$p = constant \tag{5}$$

$$\beta_t + u\beta_x + v\beta_y = w \tag{6}$$

where $z = \beta(x, y, t)$ is the free surface location.

D. Inflow Boundary Conditions

For steady-state cases, the upstream conditions are set to uniform flow ($u = U_\infty, v = 0, w = 0, \psi = 0$). For unsteady cases, a time-dependent boundary condition is prescribed. In this work we study the load of a ship moving through regular headwaves of small slope $\left(< \frac{1}{20}\right)$. Waves of this nature can be described adequately using plane progressive waves, derived under the assumptions of irrotational flow and a linearized free surface. At the inflow boundary ($x = x_o$) the following relations are prescribed for the prognostic variables

$$\beta(x_o, y, z, t) = A cos(kx_o - \omega_e t) \tag{7a}$$
$$\psi(x_o, y, z, t) = A\omega e^{kz} cos(kx_o - \omega_e t) \tag{7b}$$
$$u(x_o, y, z, t) = 1 + A\omega e^{kz} cos(kx_o - \omega_e t) \tag{7c}$$
$$v(x_o, y, z, t) = 0. \tag{7d}$$
$$w(x_o, y, z, t) = A\omega e^{kz} sin(kx_o - \omega_e t). \tag{7e}$$

Here A is the amplitude of the wave, ω is the frequency of the wave relative to a fixed reference frame, and k is the wavenumber. The frequency of encounter ω_e is defined as:

$$\omega_e = \omega + k. \tag{8}$$

E. Hull and Farfield Boundary Conditions

The remaining boundaries consist of the ship hull, the symmetry plane, and the farfield of the computational domain. In the viscous formulation, a no-slip condition is enforced on the ship hull. For inviscid (Euler) flow, tangency (no normal flow) is maintained. On the symmetry plane (that portion of the (*x,z*) plane excluding the ship hull) derivatives in the y direction as well as the v component of velocity are set to zero. On the starboard and downstream boundaries, boundary conditions are set using the method of characteristics based on the inviscid flowfield [16].

III. Numerical Solution

The formulation of the numerical solution procedure is based on a finite-volume method (FVM) for the bulk flow variables (u, v, w and ψ), coupled to a finite difference method for the free surface evolution variables (β and ψ).

A. Bulk Flow Discretization and Solution

To enforce the incompressibility constraint in a time-accurate manner, we couple the method of artificial compressibility [9] with the method of dual time-stepping. The continuity equation (Eq. 3) is augmented using the artificial preconditioning parameter Γ and an artificial time derivative in pseudotime t^*. Γ is established following the analysis of Rizzi and Eriksson [16] and further work by Turkel et al. [17]. The momentum equation (Eq. 4) is augmented with a temporal derivative in pseudotime. These modifications result in the following governing equations:

$$\frac{\partial \psi}{\partial t^*} + \Gamma^2 \frac{\partial u_i}{\partial x_i} = 0 \tag{9}$$

.

$$\frac{\partial u_i}{\partial t^*} + \frac{\partial u_i}{\partial t} + u_k \frac{\partial u_i}{\partial x_k} = -\frac{\partial \Psi}{\partial x_i} + \frac{\partial}{\partial x_k} \frac{1}{Re_t} \left(\frac{\partial u_i}{\partial x_k} + \frac{\partial u_k}{\partial x_i} \right). \tag{10}$$

With the dual-time stepping approach, equations 9 and 10 are time-marched to a steady state in pseudotime t^* at which point the system has been driven through a physical time step (Δt). The spatial derivatives are discretized using a stable centered second-order finite-volume flux formulation. The resulting system can be written as

$$P^{-1} \frac{\partial \mathbf{wV}}{\partial t^*} + T \frac{d\mathbf{wV}}{dt} + R(\mathbf{w}) = \mathbf{0}, \tag{11}$$

where $\mathbf{w} = [\psi, u, v, w]$ is the flow vector, V is the cell volume, and $R(\mathbf{w})$ is the discrete flow residual with contributions from the advection and diffusion terms as well as the pressure gradient. P is the preconditioning matrix

$$P = \begin{bmatrix} \Gamma^2 & 0 & 0 & 0 \\ 0 & 1 & 0 & 0 \\ 0 & 0 & 1 & 0 \\ 0 & 0 & 0 & 1 \end{bmatrix}, \tag{12}$$

and

$$T = \begin{bmatrix} 0 & 0 & 0 & 0 \\ 0 & 1 & 0 & 0 \\ 0 & 0 & 1 & 0 \\ 0 & 0 & 0 & 1 \end{bmatrix}. \tag{13}$$

The discrete time derivatives $\frac{d}{dt}$ of the velocity components $\frac{d\mathbf{wV}}{dt}$ are treated implicitly. The discretization is performed using a k-th order accurate backwards difference formula:

$$\frac{d}{dt} = \frac{1}{\Delta t} \sum_{q=1}^{k} \frac{1}{q} \left(\Delta^-\right)^q, \tag{14}$$

where $\Delta^- \mathbf{w}^{n+1} = \mathbf{w}^{n+1} - \mathbf{w}^n$. The resulting semi-discrete system can now be written as:

$$P^{-1} \frac{\partial \mathbf{w} V}{\partial t^*} + T \frac{1}{\Delta t} \sum_{q=0}^{k} p_q w^{n+1-q} V^{n+1-q} + R\left(\mathbf{w}^{n+1}\right) = 0. \tag{15}$$

When the system is converged in pseudotime (t^*), the equations governing incompressible viscous flow at time t^{n+1} are satisfied. Thus, the equations of motion are integrated in pseudotime to update each consecutive physical time step. The coefficients p_q for different orders of accuracy in time are summarized in table III-A.

Order of Accuracy	p_0	p_1	p_2	p_3	p_4
2	3/2	-2	1/2		
3	11/6	-3	3/2	-1/3	
4	25/12	-4	3	-4/3	1/4

TABLE I. Coefficients for backwards time difference.

By grouping together the discrete time derivative and original residual $R(\mathbf{w})$ into a single modified residual R^*, one can visualize the purpose and stability of the pseudotime iteration.

$$R^*\left(\mathbf{w}^{n+1}\right) = T \frac{1}{\Delta t} \sum_{q=0}^{k} p_q \mathbf{w}^{n+1-q} V^{n+1-q} + R\left(\mathbf{w^{n+1}}\right) = 0. \tag{16}$$

Subsequently, the semi-discrete system can be written compactly as

$$\frac{\partial \mathbf{w}^{n+1} V}{\partial t^*} + PR^*\left(\mathbf{w}^{n+1}\right) = 0. \tag{17}$$

Once the discrete system in 17 has achieved a steady-state in pseudotime (t^*), the governing equations have advanced one step in physical time Δt at the temporal accuracy of the selected backwards time difference formula.

B. Bulk Flow Solution

Equation 17 must be marched to a steady state during each physical model time step. In a typical unsteady flow calculation (see §IV) this might require 500 such solutions and therefore efficiency is critical. For this work we use a highly optimized Runge-Kutta scheme coupled with a fully nonlinear multigrid approach [18]. The full approximation multigrid scheme employs a sequence of independently generated coarser meshes by eliminating alternate points in each coordinate direction. Multigrid provides the advantage of propagating disturbances quickly on the coarser meshes and damping out the low frequency error present in the late stages of the calculation. With properly optimized coefficients, multistage time-stepping schemes can be very efficient drivers of the multigrid process. In this work we use a five stage scheme with three evaluation of dissipation [19] to drive the W cycles.

In a highly stretched, viscous mesh, the ratio of the largest to smallest time steps can be 5 orders of magnitude. Using the minimum Δt as a global time step severely hinders the convergence of the calculation. To increase the rate of convergence, the equations in each cell are advanced at a maximum cell-based time step. In general, local time-stepping destroys time accuracy. However, the modified equation set (Eq. 17) has no physical meaning until a steady state is reached.

In order to increase the allowable Courant number one can use a scheme with more stages. However, any improvements allotted by doing so are offset by the additional work required. To circumvent this problem, the residuals are smoothed using an implicit approach which requires the solution of a sequence of tridiagonal equations for each of the prognostic variables. This nominally requires a 30% increase in CPU time but allows for an increase in the allowable CFL number from 1.5 to 5.

C. Free Surface Discretization

Both a kinematic and dynamic boundary condition must be imposed at the free surface which require the adaption of the grid to conform to the computed surface waves. Since bulk flow values are stored at cell centers, they must be extrapolated up one half cell for solution of the kinematic condition. Assuming flow values are constant within a cell and applying the divergence theorem to equation 6 gives:

$$\frac{\partial}{\partial t}\int_A \beta dS + \bar{u}\oint_{\partial A}\beta dy - \bar{v}\oint_{\partial A}\beta dx = \int_A w dS \tag{18}$$

Equation 18 is discretized using a non-oscillatory scheme constructed using the Local Extremum Diminishing (LED) principle [20]. This approach allows for second order accuracy away from extrema using controlled anti-diffusion. Near sharp interfaces such as the bow-generated wave, low order dissipation is introduced locally to maintain the front. In order to maintain accuracy at smooth extrema away from the ship, a cutoff is introduced to prevent the limiter from becoming active. Formally known as essentially local extremum diminishing (ELED), this relaxed implementation of LED guarantees that maxima are non-increasing and minima are non-decreasing as $\Delta x \to 0$. This approach stabilizes the steep waves in the vicinity of the bow and shoulders of the ship while maintaining higher accuracy in the farfield and wake. Further details and results are presented in [21].

D. Free Surface Integration and Coupling with the Bulk Flow

Following the same procedure used to cast the momentum equation into a form suitable for dual time-stepping (Eq. 10), the free surface kinematic equation is expressed as

$$\frac{d\beta_{ij}}{dt^*} + Q_{ij}(\beta) = 0 \tag{19}$$

where $Q_{ij}(\beta)$ consists of the collection of vertical velocity and spatial and temporal gradient terms which result from the discretization of equation 18. The free surface is integrated with a three-stage explicit Runge-Kutta algorithm with dissipation evaluations on all stages.

Once the free surface update is accomplished, the pressure is adjusted on the free surface such that

$$\psi(x,y) = \beta(x,y)Fr^{-2}. \tag{20}$$

The free surface and the bulk flow solutions are coupled by first computing the bulk flow at each time step, and then using the bulk flow velocities to calculate the movement of the free surface. After the free surface is updated, its new values are used as a boundary condition for the pressure on the bulk flow for the next time step. The entire iterative process, in which both the bulk flow and the free surface are updated at each time step, is repeated until some measure of convergence is attained: usually steady state wave profile and wave resistance coefficient.

The coupled flow solver is parallelized using a Single Program Multiple Data (SPMD) approach with communication between processors programmed using the MPI standard. Discretization of dissipative fluxes for the bulk flow and free surface require the establishment of a two level halo for interprocessor exchanges.

IV. Results

The solver presented in this work is used to compute the added resistance of a ship moving through regular headwaves. In his experiments, Journée [22] measured the time-dependent resistance as well as hull orientation (sink and trim) for 4 Wigley hulls in regular head waves of varying amplitude and wavelength. For demonstration of the time-dependent flow solver, one particular case is selected. The experimental parameters for a representative test case are shown in Table II. This case was chosen from the extensive experimental set because the disparity between body wave amplitude and external wave amplitude generates nonlinear interaction between the two fields.

TABLE II. Experimental Conditions for Test Case

Ship		External Wave	
Froude	Re $\times 10^{-6}$	Length λ_w/L	Amplitude A/L
0.3	4.86	1.0	.0083

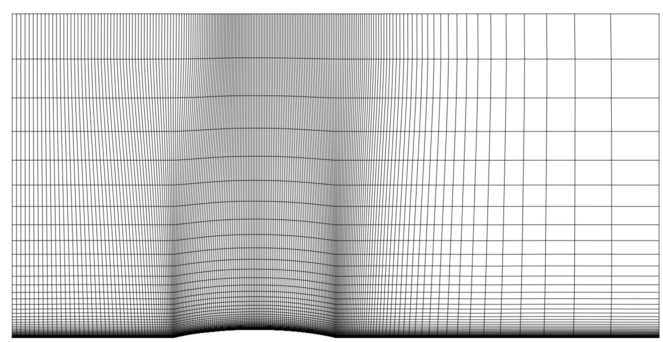

Fig. 2. Free Surface of Unsteady Wigley III Mesh

A. Numerical Setup

The choice of initial condition influences the time required to reach a periodic solution. Reduction of the transient time represents a savings in computational costs which can be quite large in these unsteady flows. The initial condition utilized for this work was constructed by adding together the steady solution for the given Froude and Reynolds numbers with the analytical solution for the plane progressive wave. This was performed for all of the flow variables u_i, ψ and β. For the second-order time-stepping, two time levels are required to initialize the flow solver. With this method, the transient is seen to decay within four periods of the external wave field. The amplitude and phase of the first Fourier mode of resistance does not change more than 1% between $t = 3T$ and $t = 5T$ where T is the period of the external wave.

$$T = \frac{2\pi}{\omega} \tag{21}$$

For these computations, a baseline mesh was established. The mesh contains 193 points in the streamwise direction, 65 points to starboard and 33 points normal to the free surface (Fig. 2). The grid spacing normal to the hull was based on a y^+ value of unity for the corresponding Reynolds number based on hull length. For this case, $\Delta S/L = 5.42 \times 10^{-6}$.

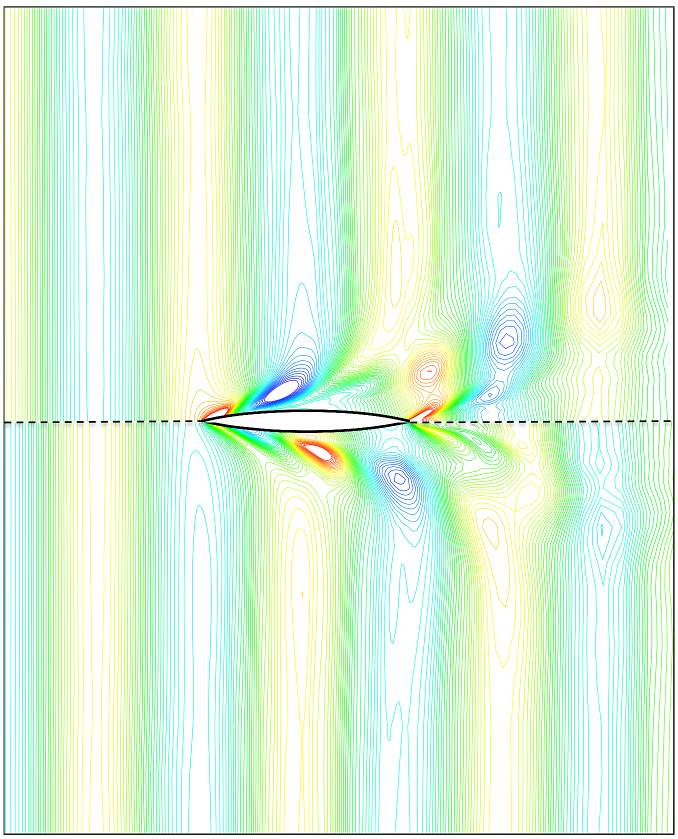

Fig. 3. Unsteady free surface elevation contours: upper panel (t = T) and lower panel ($t = T/2$)

B. Comparison with Experiment

Comparison of computed and measured steady state and time-dependent coefficients of the resistance modes are shown in Table III. Resistance is normalized by $\frac{1}{2}\rho S_{wet} U^2$ where S_{wet} is the wetted area. The resistance components are decomposed into harmonics of the form:

$$R(t) = R_m + \sum_{k=1}^{p} R_n cos\left[k\omega_e t + \gamma(R_n)\right] \tag{22}$$

Only the amplitude and phase of the first mode are reported in the experimental data of Journée. The amplitudes of the higher modes are negligible. Table III shows a comparison between the computed and measured amplitudes and modes for the test conditions in Table II using the baseline 193x65x33 mesh. The phase lag (γ_J) reported experimentally is relative to the wave elevation at the center of gravity of the ship model. The phase as calculated in equation 22 is shifted forward 180° to match this definition. Error in the amplitude is 5%, while error in phase is 3°. Observational error was not reported for either measurement.

TABLE III. COMPARISON OF COMPUTATION AND EXPERIMENT: RESISTANCE AMPLITUDE AND PHASE

	Amplitude $\times 10^{-3}$		Phase	
Mode	Comp	Exp	Comp	Exp
Steady	5.51	5.59	-	-
1	5.12	5.39	112	109
2	.09	-	135	-
3	.02	-	130	-

C. Grid and Time Refinement

In Table IV, the first mode amplitude and phase are provided for various mesh sizes. Using the coarse resolution 129x65x25 mesh, the error in amplitude prediction jumps to 9% when compared to the experiment. The phase, however, agrees very well with the experimental value. Altering the grid dimensions from the baseline 193x65x33 to the finer 257x65x49 does not appreciably change either the amplitude or phase calculation.

TABLE IV. MODE 1 AMPLITUDE AND PHASE VS. GRID SIZE

Mesh	Mode 1 Amp	Mode 1 Phase
129x65x25	4.87×10^{-3}	109
193x65x33	5.12×10^{-3}	112
257x65x49	5.12×10^{-3}	111

In Table V, the first mode amplitude and phase are provided for various temporal resolutions using the 193x65x33 mesh. Using 48 time steps in each external wave period, the error in amplitude is roughly 8%. With an increase from 72 to 96 time steps per period, the error remains roughly fixed at 5% while the phase is unaltered.

TABLE V. MODE 1 AMPLITUDE AND PHASE VS. TIME STEP

Steps/T	Mode 1 Amp	Mode 1 Phase
48	4.93×10^{-3}	111
72	5.09×10^{-3}	112
96	5.12×10^{-3}	111

Figure 3 shows the free surface elevation during two phases of a wave period. Figure 4 displays the waterline during these two wave phases along with the steady state waterline for reference. The nonlinear interaction between the wave components is clear.

D. Computational Requirements

The computational work required for the time-dependent solution is approximately two orders of magnitude larger than that required for the steady solution at the same *Fr* and *Re*. For example, approximately 400 multigrid cycles are needed to achieve a steady state solution of the Wigley hull at $Fr = .3$ and $Re = 4.86 \times 10^6$. A typical unsteady solution requires 5 periods of physical time with 72 time steps in each period and 80 multigrid cycles per time step for a total of $28,800$ multigrid cycles, a factor of 72 greater than the steady state case. A calculation on the baseline 193x65x33 mesh requires approximately one minute of compute time on 16 Intel Nehalem cores for the steady case and 90 minutes for the unsteady case.

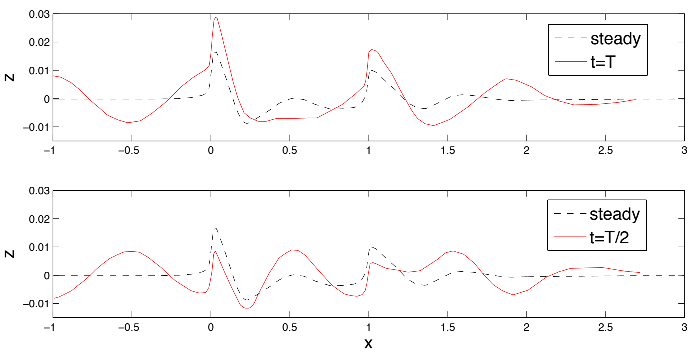

Fig. 4. Waterlines: upper panel (t = T) and lower panel ($t = T/2$) with steady waterline (dashed) for reference

V. Conclusions

In the present work, a numerical method for simulating viscous flows with a free surface for general hullforms was presented. The solver can be used to simulate both steady and time-dependent flows past surface-piercing and submerged bodies. Fast convergence rates of the solver are obtained by coupling a nonlinear multigrid method with local time-stepping and residual smoothing. For unsteady flows, the method of dual-time stepping is employed whereby the flow residual is augmented with the discrete temporal derivative using a point implicit approach. This method enables straightforward selection of temporal order of accuracy and stability. The comprehensive flow solver is parallelized using a single program multiple domain (SPMD) approach with MPI and achieves good scalability on modern distributed computing systems.

Comparison with measurement from tank testing is used to demonstrate the capability of the method. The flow solver accurately reproduces the total resistance of a Wigley hull traveling at steady speed through quiescent flow as well as through regular headwaves. The solver reproduces well the amplitude and phase of the first mode of the time-dependent invariant flow. A grid convergence study was carried out to examine the influence of resolution on the calculated resistance. A mesh size of 193x65x33 (393,216 control volumes) was needed to satisfy resistance coefficient of the first mode to two digits.

References

[1] T. Hino, "Computation of a free surface flow around an advancing ship by the Navier-Stokes equations." 5th International Conference Numerical Ship Hydrodynamics, 1989.

[2] H. Miyata, T. Sato, and N. Baba, "Difference solution of a viscous flow with free-surface wave about an advancing ship," *Journal of Computational Physics*, vol. 72, pp. 393–421, 1987.

[3] Y. Tahara, F. Stern, and B. Rosen, "An interactive approach for calculating ship boundary layers and wakes for nonzero Froude number," *Journal of Computational Physics*, vol. 98, pp. 33–53, 1992.

[4] J. Farmer, "A finite volume multigrid solution to the three dimensional nonlinear ship wave problem," Ph.D. dissertation, Princeton University, Department of Mechanical and Aerospace Engineering, January 1993.

[5] N. Salveson, E. Tuck, and O. Faltinsen, "Ship motions and sea loads," *SNAME Transactions*, vol. 78, 1970.

[6] *WAMIT Version 2.1, A Radiation-Difraction Panel Program for Wave-Body Interactions*, Dept. of Ocean Engineering, Massachusetts Institute of Technology, Cambridge, MA.

[7] S. Rhee and F. Stern, "Unsteady RANS method for surface ship boundary layer and wake and wave field," *Intl. Journal for Numerical Methods in Fluids*, vol. 37, pp. 445–478, 2001.

[8] L. Martinelli and A. Jameson, "An adjoint method for design optimization of ship hulls." Ann Arbor, MI: 9th International Conference on Numerical Ship Hydrodynamics, 2007.

[9] A. J. Chorin, "A numerical method for solving incompressible viscous flow problems," *J. Comp. Phys.*, vol. 2, pp. pp. 12–26, 1967.

[10] R. Peyret, "Unsteady evolution of a horizontal jet in a stratified fluid," *Journal of Fluid Mechanics*, vol. 78, pp. 49–63, 1976.

[11] A. Jameson, "Time dependent calculations using multigrid, with applications to unsteady flows past airfoils and wings," AIAA 10th CFD Conference, Honolulu, HI, *AIAA paper 91-1596*, June 1991.

[12] J. J. Alonso, "Parallel computation of unsteady and aeroelastic flows using an implicit multigrid driven algorithm," Ph.D. dissertation, Princeton University, June 1997.

[13] A. Belov, "A new implicit multigrid-driven algorithm for unsteady incompressible flow calculations on parallel computers," Ph.D. dissertation, Princeton University, Department of Mechanical and Aerospace Engineering, June 1997.

[14] P. Lin, L. Martinelli, and T. Baker, "Two-dimensional implicit time dependent calculations for incompressible flows on adaptive unstructured meshes," AIAA 15th Computational Fluid Dynamics Conference, Anaheim, CA, *AIAA paper 2001-2655*, June 2001.

[15] B. Baldwin and H. Lomax, "Thin layer approximation and algebraic model for separated turbulent flows," AIAA 16th Aerospace Sciences Meeting, Reno, NV, *AIAA paper 78-257*, January 1978.

[16] A. Rizzi and L.-E. Eriksson, "Computation of inviscid incompressible flow with rotation," *J. Fluid Mech.*, vol. 153, no. pp. 275-312, 1985.

[17] E. Turkel and A. Arnone, "Pseudo-compressibility methods for the incompressible flow equations," Institute for Computer Applications in Science and Engineering, NASA Langley Research Center, ICASE Report 93-66, September 1993.

[18] A. Jameson, "Multigrid algorithms for compressible flow calculations," in *Lecture Notes in Mathematics, Vol. 1228*, W. Hackbusch and U. Trottenberg, Eds., Proceedings of the 2nd European Conference on Multigrid Methods, Cologne, 1985. Springer-Verlag, 1986, pp. 166–201.

[19] L. Martinelli, "Calculation of viscous flows with a multigrid method," Ph.D. dissertation, Princeton University, Department of Mechanical and Aerospace Engineering, October 1987.

[20] A. Jameson, "Analysis and design of numerical schemes for gas dynamics 1, artificial diffusion, upwind biasing, limiters and their effect on multigrid convergence," *Int. J. of Comp. Fluid Dyn.*, vol. 4, pp. 171–218, 1995.

[21] J. Farmer, L. Martinelli, A. Jameson, and G. Cowles, "Fully-nonlinear CFD techniques for ship performance analysis and design," AIAA 12th Fluid Dynamics Conf, San Diego, CA, *AIAA paper 95-1690*, June 1995.

[22] J. Journée, "Experiments and calculations on four wigley hullforms," Delft University of Technology, Ship Hydromechanics Laboratory, *Technical Report 909*, 1992.